Published OnlineFirst November 14, 2018; DOI: 10.1158/1541-7786.MCR-18-0138

Molecular Cancer Research

PARP1 Trapping by PARP Inhibitors Drives Cytotoxicity in Both Cancer Cells and Healthy Bone Marrow

Todd A. Hopkins, William B. Ainsworth, Paul A. Ellis, Cherrie K. Donawho, Enrico L. DiGiammarino, Sanjay C. Panchal, Vivek C. Abraham, Mikkel A. Algire, Yan Shi, Amanda M. Olson, Eric F. Johnson, Julie L. Wilsbacher, and David Maag

Abstract

PARP inhibitors have recently been approved as monotherapies for the treatment of recurrent ovarian cancer and metastatic *BRCA*-associated breast cancer, and ongoing studies are exploring additional indications and combinations with other agents. PARP inhibitors trap PARP onto damaged chromatin when combined with temozolomide and methyl methanesulfonate, but the clinical relevance of these findings remains unknown. PARP trapping has thus far been undetectable in cancer cells treated with PARP inhibitors alone. Here, we evaluate the contribution of PARP trapping to the tolerability and efficacy of PARP inhibitors in the monotherapy setting. We developed a novel implementation of the proximity ligation assay to detect chromatin-trapped PARP1 at single-cell resolution with higher sensitivity and throughput than previously reported methods. We further demonstrate that the PARP inhibitor–induced trapping appears to drive single-agent cytotoxicity in healthy human bone marrow, indicating that the toxicity of trapped PARP complexes is not restricted to cancer cells with homologous recombination deficiency. Finally, we show that PARP inhibitors with dramatically different trapping potencies exhibit comparable tumor growth inhibition at MTDs in a xenograft model of *BRCA1*-mutant triple-negative breast cancer. These results are consistent with emerging clinical data and suggest that the inverse relationship between trapping potency and tolerability may limit the potential therapeutic advantage of potent trapping activity.

Implications: PARP trapping contributes to single-agent cytotoxicity of PARP inhibitors in both cancer cells and healthy bone marrow, and the therapeutic advantage of potent trapping activity appears to be limited.

Introduction

The recent approvals of the PARP inhibitors olaparib (Lynparza) and rucaparib (Rubraca) for the treatment of *BRCA*-mutated ovarian cancer (1) and niraparib (Zejula) for the treatment of recurrent ovarian cancer with or without *BRCA* mutation (2) are important benchmarks in over 50 years of research since the initial discovery of this important class of enzymes. The enzymatic function of PARP1, known as PARylation, is the synthesis of ADP-ribose polymers (PAR) that covalently modify host proteins or its own automodification domain (3). When DNA is damaged, PARP1 binds the damage site and catalyzes synthesis of PAR that recruits host DNA repair proteins. AutoPARylation of PARP1 induces an electrostatic destabilization and dissociation from the DNA damage site which enables repair proteins to localize to the lesion (4, 5). As a result, DNA damage is repaired, and cell viability is maintained. When DNA damage occurs in the presence of a PARP inhibitor, PARP1 binds to damage sites and remains tightly bound or trapped onto the chromatin. PARylation is inhibited, and PARP1 remains bound to the lesion, which progresses to replication fork collapse and DNA double-strand breaks (DSB; ref. 6). In homologous recombination (HR)–competent cells, DNA damage is repaired by the HR pathway, and cells remain viable. In HR-defective (HRD) cells such as *BRCA* 1/2 mutants, DSB damage is not repaired with high fidelity, resulting in cell death. The cytotoxicity induced by the combination of HRD and PARP inhibitors is known as synthetic lethality (1).

There are now more than 150 completed, running, or planned registered trials for the PARP inhibitors niraparib, olaparib, rucaparib, talazoparib, and veliparib (www.clinicaltrials.gov). The majority of these trials are monotherapy studies in patients with tumors harboring DNA repair defects, whereas the remaining trials are combinations with chemotherapies including platinums, taxanes, ATM inhibitors, ATR inhibitors, Wee1 inhibitors, and PI3K inhibitors as well as with immune-oncology therapies. The role of PARP trapping in the efficacy of clinical PARP inhibitors is under intensive investigation. *In vitro* studies in DT40 cells showed that all five clinical PARP inhibitors were able to potentiate DNA damage induced by alkylating agents, and knockout of PARP1 eliminated this effect (7, 8). Although there is only a 40-fold difference in IC_{50}s between the most potent (talazoparib) and least potent (veliparib) compound in catalytic inhibition studies, the difference in PARP trapping activity between the inhibitors was greater than 10,000-fold (9). This differential

AbbVie, Inc., North Chicago, Illinois.

Note: Supplementary data for this article are available at Molecular Cancer Research Online (http://mcr.aacrjournals.org/).

Corresponding Author: David Maag, AbbVie, Inc., 1 N. Waukegan Road, Dept R460, Bldg AP30-3, North Chicago, IL 60064-6122. Phone: 847-937-3969; Fax: 847-935-5165; E-mail: David.Maag@abbvie.com

doi: 10.1158/1541-7786.MCR-18-0138

Published OnlineFirst November 14, 2018; DOI: 10.1158/1541-7786.MCR-18-0138

trapping potency was theorized to be the result of an allosteric change in protein conformation induced by the more potent trapping agents (7, 8); however, we found no evidence of allostery after rigorous biochemical testing (9). Thus, the underlying mechanism behind the high trapping potency of talazoparib relative to other PARP inhibitors remains to be determined.

The importance of PARP trapping to the cytotoxic mechanism of PARP inhibitors appears to be context dependent. Although the activity of PARP inhibitor combinations with temozolomide appear to be mediated largely by PARP trapping, in the context of combinations with other DNA-damaging agents like platinums and irinotecan, efficacy appears to be less dependent on PARP1 trapping (10). The importance of PARP1 trapping in the monotherapy setting remains equivocal. Genetic evidence and correlations with preclinical and clinical MTDs suggest that trapping occurs in this context (7–9), but it has yet to be demonstrated directly.

In this study, we sought to better understand the effects of PARP1 trapping on PARP inhibitor tolerability and efficacy in the monotherapy setting. To assess the properties of PARP inhibitors that contribute to efficient trapping, we characterized a panel of compounds with similar catalytic potencies and PARP-binding residence times to the potent PARP trapping agent talazoparib. This includes the first reported characterization of a novel PARP inhibitor, A-934935. Utilizing a highly sensitive proximity ligation assay (PLA), we were able to detect chromatin-trapped PARP at single-cell resolution following single-agent PARP inhibitor treatment. Kinetics of PARP trapping relative to PAR inhibition, DNA damage induction, and apoptosis were also analyzed. In addition, PARP inhibitor cytotoxicity was determined in bone marrow (BM) progenitors to evaluate contributions of trapping to BM toxicity observed in the clinic. Our data suggest an inverse relationship between PARP inhibitor trapping potency and tolerability due to cytotoxicity within normal cells, and provide important context for translation of reported *in vitro* trapping activity differences to clinical outcomes.

Materials and Methods

Cell culture

HeyA8 cells purchased from M.D. Anderson were maintained in RPMI 1640 with 10% FBS at 5% CO_2 and 37°C. Isogenic DLD1 and DLD1-*BRCA2*$^{-/-}$ cells with homozygous deletion of *exon 11* of *BRCA2* were maintained in RPMI 1640 with 10% FBS at 5% CO_2 and 37°C. Isogenic haploid cell line HAP1 and HAP1 *PARP1* knockout cells were maintained in Iscove's Modified Dulbecco's Medium (IMDM) with 10% FBS at 5% CO_2 and 37°C. DLD1 and HAP1 lines were licensed from Horizon Discovery, Ltd. Cell lines H69, H1048, H1930, H2081, T47D, UACC812, and MDA-MB-436 were purchased from the ATCC. SUM149PT was purchased from Asterand Bioscience. All cell lines were authenticated immediately prior to freezing aliquots between October of 2013 and January of 2015 using the Promega GenePrint 10 system. Cells were used within 40 passages after thawing. SUM149PT cells for *in vivo* studies were grown to passage 3 *in vitro* in RPMI (Life Technologies) containing 10% FBS (Hyclone) and harvested while in log phase.

High-content imaging of γH2A.X, caspase 3/7, and cellular PLAs

Cells were plated in 96-well collagen I–coated Costar plates (Corning; cat# 356649) at densities to achieve 90% confluence at time of fixation. Veliparib, olaparib, and talazoparib were synthesized as previously described (9). Rucaparib was synthesized using published methods (11) or purchased from Selleckchem. A-934935 was synthesized using methods disclosed in ref. 12. Compounds were diluted in DMSO, serial diluted in DMSO, and added to cell plates at indicated concentrations with final DMSO concentrations <0.1%. Cells were fixed with 2% formaldehyde (Polysciences; #04018) for 10 minutes, permeabilized with 0.1% Triton X-100 in 1xPBS for 10 minutes, and blocked in 2% BSA for 1 hour with washes in 1xPBS between each step. Cells were treated with indicated antibodies at a 1:400 dilution in antibody dilution buffer (0.3% BSA in 1xPBS) at 4°C overnight. Antibodies used for H2A.X and PLA include PARP-1 mAb (Sigma; #WH0000142M1), PARP1, Histone H2B, total H2A.X and γH2A.X (Cell Signaling Technology; #9542, #12364, #7631, and #9718), NPM1, KAP1, Histone H3, and Histone H4 (Bethyl; #A302-404A, #A300-274A, #A300-823A, and #A300-646A), Lamin A/C (Invitrogen; #MA3-1000), and BRCA1 (Gentex; #GTX70111).

Cell imaging. For γH2A.X, cells were washed 3x in PBS and incubated with Alexa Fluor 488–conjugated goat anti-rabbit Ab (Life Technologies; #A11034) and Hoechst 33342 (Life Technologies; # H2570) diluted 1:400 and 1:8,000, respectively, in antibody dilution buffer for 1 hour at room temperature. Plates were washed 3x with PBS and scanned using 10x objective within 24 hours. For caspase 3/7, samples were treated with CellEvent Green Caspase 3/7 Detection Reagent (Molecular Probes; #C10423) in complete media at a final concentration of 2 μmol/L for 24 hours prior to fixation. Cells were fixed, permeabilized, and treated with Hoechst as previously described. Plates were washed and scanned immediately using 10x objective on a CellInsight.

Duolink PLA. The Duolink Proximity Ligation Assay was performed per the manufacturer's protocol (Sigma; DUO92008-100RXN, DUO92004-100RXN, and DUO92002-100RXN). Labeling of nuclear DNA was performed in antibody dilution buffer with Hoechst 33342 at 2 μmol/L. Final reaction plates were washed 3X with PBS and scanned within 24 hours by automated image acquisition using a 20x objective on a CellInsight. Image analysis was performed on the CellInsight HCS Reader, and data analysis was performed using Cellomics View Software. Graphs are the mean and standard errors of duplicate samples tested in at least three independent experiments.

Cellular and biochemical assays

Cellular trapping, cell viability, PAR ELISA, and TR-FRET–binding assays were performed as previously described (9). Biochemical assays for the specified PARP family of enzymes were conducted at BPS Bioscience Inc.

Equilibrium binding and kinetic studies of PARP1–PARP inhibitor complexes

Biacore assays were performed as previously described (9) with the following modification: Analysis used single-cycle kinetics mode in 5-point and 3-fold concentration series from 0.62 nmol/L to 50 nmol/L (talazoparib) or 1.1 nmol/L to 90 nmol/L (A-934935 and rucaparib), respectively.

BM PAR assay

Frozen BM mononuclear cells were purchased from Lonza (cat# 2M-125C). Cultures were thawed per manufacturer protocol.

Published OnlineFirst November 14, 2018; DOI: 10.1158/1541-7786.MCR-18-0138

Cells were maintained in IMDM + 2%FBS + supplemented with StemSpan CC100 bullet (Stemcell Technologies; cat# 02690). Cells were plated in complete media at a density of 7×10^5 cells per well and treated with compounds for 5 days. Cellular PAR levels were measured by ELISA as described (13–15).

BM colony formation assays

All BM colony formation assays were conducted at StemCell Technologies. Normal human BM lot BM070525B, lot BM10A33225, and lot BM070973A (Lonza) were thawed rapidly at 37°C into DNaseI, then diluted into 10 mL of IMDM + 2% FBS, and washed by centrifugation. The resulting cell pellet was resuspended into IMDM + 2% FBS. Hematopoietic cultures were plated in triplicate at a density of 1×10^4 cells per dish in MethoCult media (Stemcell Technologies, MethoCult cat# GF H84434). Compounds were diluted to make 1,000X stocks in DMSO followed by further dilution into MethoCult to achieve final concentrations. Cultures were incubated for 13 to 16 days at 37°C at 5% CO2. Mean colony numbers following compound treatment were used to calculate IC_{20}, IC_{50}, and IC_{90} values using GraphPad Prism 5 software.

In vivo pharmacology

Determination of MTDs. Animal research was approved and overseen by the AbbVie Institutional Animal Care and Use Committee [in accordance with all Association for Assessment and Accreditation of Laboratory Animal Care (AAALAC) guidelines]. Veliparib, olaparib, and talazoparib formulations were prepared as previously described (6). Tolerability studies were conducted in naïve C.B-17 SCID female mice. Talazoparib was dosed p.o. qd, and other PARP inhibitors were administered p.o., b.i.d. for 21 days. Doses resulting in <15% weight loss were considered tolerable.

SUM149PT xenograft models. SUM149PT cells (2×10^6) in 0.1 mL of a 1:1 mixture of S-MEM (Life Technologies) and Matrigel (Corning) were inoculated subcutaneously into the right flank of female C.B-17 SCID mice (Charles River Laboratories) on day 0.

Efficacy studies. SUM149PT xenografts were size matched on day 29 with a mean tumor volume of 235 ± 14 mm^3 and dosed starting on day 30. Ten mice per group were treated with the indicated oral doses of PARP inhibitors administered b.i.d. for vehicle, veliparib, olaparib, and qd for talazoparib, for 42 days. Mice were observed daily, and tumors were measured 2 times per week. When tumor volumes reached a maximum of 2,500 mm^3 or when skin ulcerations occurred, mice were euthanized. Electronic calipers were used to measure tumor length (L) and width (W), and tumor volume was calculated according to the following equation: $V = L \times W^2/2$ using Study Director version 3.1 (Studylog Systems, Inc.).

Pharmacokinetics and pharmacodynamics. SUM149PT tumor-bearing mice were size matched and treated with the same doses and schedules as for the efficacy study but only for 5 days. Plasma and tumor samples were collected at 1, 4, 24, 32, and 48 hours following the final dose. Blood samples were collected in microtainer tubes (BD bioscience) containing K^+-EDTA and centrifuged. The upper layer, consisting of the plasma, was collected and frozen. Tumor samples were flash frozen in liquid nitrogen. Inhibitor (16) and PAR levels (13–15) were measured as described.

Results

Evaluation of trapping vs. catalytic inhibition for compounds that are equipotent to talazoparib

Studies have shown that PARP inhibitors with similar catalytic potency can differ in their ability to induce PARP1 trapping (6, 8); however, the unique potency and binding residence time exhibited by the PARP inhibitor talazoparib confound interpretation of the relationship between trapping and cytotoxic potency. Given the differential resolution between catalytic inhibition and trapping of PARP inhibitors, we sought to identify compounds that inhibit PARP1 equipotently to talazoparib while exhibiting a much greater resolution between catalytic inhibition and trapping activities. Rucaparib and a proprietary PARP inhibitor, A-934935, were identified as compounds with similar binding properties as talazoparib, as determined by surface plasmon resonance (Fig. 1A). Talazoparib, rucaparib, and A-934935 also inhibit PARP1 activity in cells equipotently, with IC_{50} values of 3, 9, and 4 nmol/L, respectively (Fig. 1B) and trap full length PARP1 in a biochemical system identically with EC_{50} values of 2, 2, and 4 nmol/L, respectively (Fig. 1C). Despite these similarities, talazoparib produces substantially more PARP1 trapping and DNA damage potentiation activities in cells treated with methyl methanesulfonate (MMS; Fig. 1D and E). These results indicate that the potent trapping and DNA-damaging activities of talazoparib are not simply attributable to PARP1-binding properties. Although these data would be consistent with the proposed allosteric trapping hypothesis (7), a rigorous biochemical investigation revealed no evidence of allosteric trapping for talazoparib (9). Moreover, the unique trapping efficiency of talazoparib relative to rucaparib and A-934935 is only evident in intact cells, whereas any potential unique allosteric trapping activity would be expected to manifest in biochemical trapping assays (Fig. 1C).

To investigate whether these differences in PARP inhibitor trapping activity and DNA damage potentiation were due to variability in polypharmacology, the compounds were characterized for inhibition of other PARP family members using biochemical activity assays for 12 of the 17 PARP family members (Supplementary Table S1). In comparison to PARP1 and PARP2, the role of other PARP family members in DNA damage repair and the cytotoxicity of different PARP inhibitors has not yet been well established. Talazoparib, rucaparib, and A-934935 were equipotent inhibitors of PARP1/2. Relative to their PARP1/2 IC_{50}s, rucaparib was approximately 100-fold less potent against PARP3, talazoparib was approximately 100-fold less potent against PARP3, TNKS1, and TNKS2, and A-934935 was approximately 100-fold less potent against TNKS2. All three compounds were inactive against PARP6, 7, 8, 10, 11, 12, and 15. Although talazoparib displayed somewhat unique potency at inhibiting TNKS1 and TNKS2, this did not appear sufficient to account for the potency with which the compound potentiates DNA damage or traps PARP1.

Cytotoxicity of talazoparib is driven by PARP1

Avian cells such as DT40 are naturally *PARP2* deficient, and knockout of *PARP1* expression results in loss of cytotoxicity to single-agent PARP inhibitor treatments (7, 8). We performed analogous experiments utilizing a *PARP2*-proficient HAP1 cell line with CRISPR/Cas9-generated *PARP1* knockout (HAP1 *PARP1* KO). Talazoparib, rucaparib, and A-934935 showed decreased cytotoxicity in the HAP1 *PARP1* KO cells relative to the isogenic HAP1 wild-type (HAP1 WT) cells. If inhibition of PARP1 catalytic

Published OnlineFirst November 14, 2018; DOI: 10.1158/1541-7786.MCR-18-0138

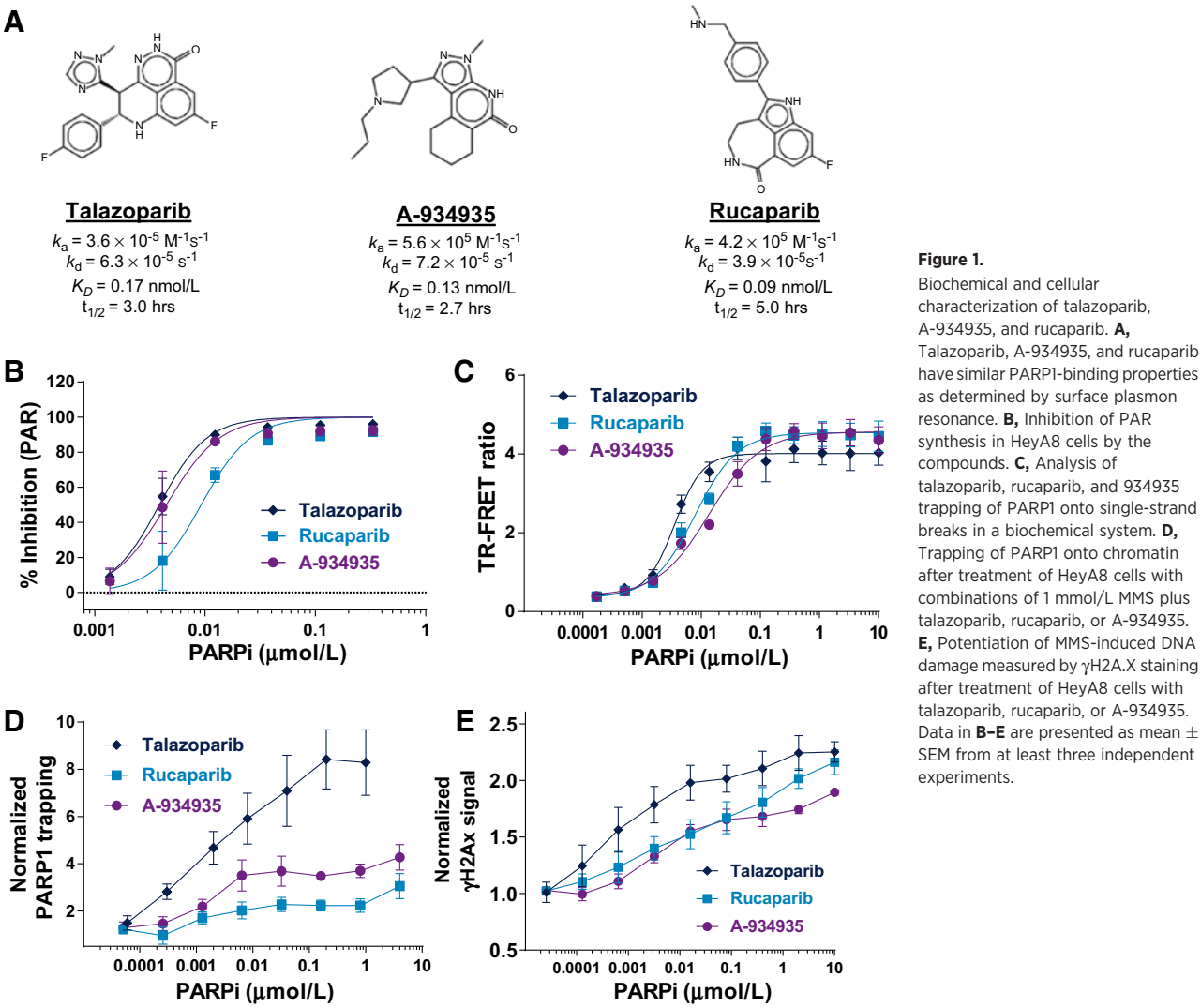

Figure 1.
Biochemical and cellular characterization of talazoparib, A-934935, and rucaparib. **A,** Talazoparib, A-934935, and rucaparib have similar PARP1-binding properties as determined by surface plasmon resonance. **B,** Inhibition of PAR synthesis in HeyA8 cells by the compounds. **C,** Analysis of talazoparib, rucaparib, and 934935 trapping of PARP1 onto single-strand breaks in a biochemical system. **D,** Trapping of PARP1 onto chromatin after treatment of HeyA8 cells with combinations of 1 mmol/L MMS plus talazoparib, rucaparib, or A-934935. **E,** Potentiation of MMS-induced DNA damage measured by γH2A.X staining after treatment of HeyA8 cells with talazoparib, rucaparib, or A-934935. Data in **B–E** are presented as mean ± SEM from at least three independent experiments.

activity is the exclusive driver of cytotoxicity in a particular cellular context, then all three compounds should be equipotent in cytotoxicity assays, yet talazoparib displayed significantly greater cytotoxic potency than either rucaparib or A-934935 in HAP1 WT cells (Fig. 2). Knockout of *PARP1* in HAP1 cells resulted in modest 4-fold and 11-fold increases in IC_{50} for rucaparib and A-934935, suggesting that the PARP1 trapping activities of these compounds are sufficient to contribute to single-agent cytotoxicity (Fig. 2). In contrast, the cytotoxic potency of talazoparib is reduced by over 300-fold in HAP1 *PARP1* KO cells, suggesting that PARP1 trapping is the primary driver of the cytotoxicity of this compound (Fig. 2). Collectively, these data suggest that PARP1 trapping is an important driver of PARP inhibitor cytotoxicity in the monotherapy setting, and that talazoparib is unique in the extent to which trapping drives cytotoxic potency.

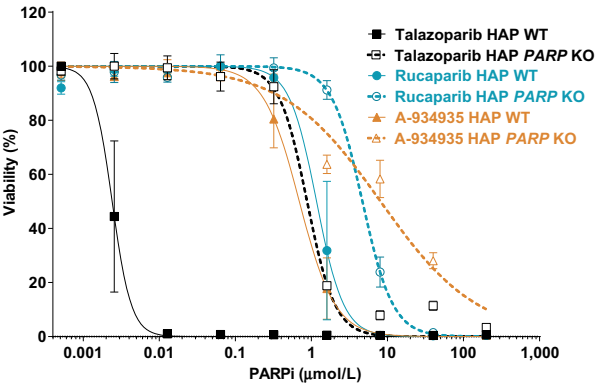

Figure 2.
Cytotoxicity of talazoparib is driven by PARP1. Cell viability dose–response curves for talazoparib, A-934935, and rucaparib following treatment of HAP1 wt and HAP1 *PARP1* knockout cells for 5 days. Data points are mean ± SEM from three independent experiments.

Direct evidence of PARP1 trapping after single-agent treatment of cancer cells with PARP inhibitors

It has been well documented that alkylating agent combinations with PARP inhibitors induce PARP1 trapping to chromatin (7–10); however, detection of single-agent PARP inhibitor–

Published OnlineFirst November 14, 2018; DOI: 10.1158/1541-7786.MCR-18-0138

induced trapping has not been shown. Established methods to detect PARP1 trapping, such as subcellular fractionation followed by Western detection, have several limitations including low throughput, potential loss of trapped complexes during processing, non-native conditions, and insufficient sensitivity for detecting trapping induced by PARP inhibitor monotherapy. To address these pitfalls, we utilized a highly sensitive, fluorescence-based PLA to detect trapped PARP1 at the single-cell level. Histone H2A.X is an abundantly expressed, chromatin-associated protein that is phosphorylated at Ser139 (also known as γH2A.X) upon DNA damage. Previous combination studies with alkylating agents and PARP inhibitors have shown enhancement of γH2A.X signal (9); we therefore theorized that under DNA-damaging conditions PARP1 and total H2A.X (tH2A.X) would associate within the 40 angstrom distance required for PLA ligation and amplification reactions. Treatment of DLD-1 cells with 1 mmol/L MMS and 0.1 μmol/L talazoparib followed by PLA staining with antibody pairs PARP1/tH2A.X or PARP1/γH2A.X resulted in robust PLA signal (Supplementary Fig. S1A and S1B). This signal strongly correlates with data generated with previously established fractionation and Western blot methods, and recapitulates the reported rank order of weaker trapping by veliparib relative to stronger trapping by talazoparib (refs. 7–9; Supplementary Fig. S1C and S1D). The PLA signal for γH2A.X was higher than that observed for total H2A.X (Supplementary Fig. S1A and S1B). Total loss of PLA signal was observed if PARP1, tH2A.X, or γH2A. X antibodies were removed individually from the PLA reaction. The PLA signal appears limited to specific partner proteins, as much weaker signal was observed with Histone H2B and Histone H3 (Supplementary Fig. S2), and no signal was observed with Histone H4, NPM1, KAP1, Lamin A/C, or BRCA1 (data not shown), although it cannot be ruled out that some of these antibodies are simply inadequate for the method. The total H2A.X antibody was chosen for further experiments because it produces a robust signal when paired with PARP1, and its abundance is not dependent on DNA damage (which may confound interpretation of results).

To investigate the cytotoxic role of PARP trapping following PARP inhibitor monotherapy, we treated the HR-proficient cell line DLD wild-type (DLDwt) and two HR-deficient cell lines DLD *BRCA2*$^{-/-}$ and SUM149PT (a *BRCA1*-mutant triple-negative breast cancer line) with increasing concentrations of veliparib in a time course study. In all three cell lines, there was a dose-dependent inhibition of PAR formation, indicating inhibition of PARP1 catalytic activity (Fig. 3A–C). In DLD *BRCA2*$^{-/-}$ and SUM149PT cells, a time-dependent synthetic lethality was observed (Fig. 3E and F) with concordant increases in γH2A.X-associated DNA damage, caspase 3/7 activity, and PLA signal (Fig. 3B and C). These data are consistent with previously reported PARP inhibitor concentrations that inhibit greater than 95% of PAR formation and induce PARP1 trapping in combination with alkylating agents (9). In the DLDwt cell line, PAR was depleted to similar levels as in DLD *BRCA2*$^{-/-}$ cells; however, no dose-dependent increases in γH2AX associated DNA damage, caspase 3/7 activity, or PLA signal were observed (Fig. 3A). Likewise, veliparib monotherapy did not induce cytotoxicity in the DLDwt lines (Fig. 3D).

PARP1 trapping drives cytotoxicity in BM

Using the set of PARP inhibitors with identical PAR inhibition potencies but dramatically different trapping potencies, we sought to understand the significance of potent trapping activity for the tolerability and efficacy of PARP inhibitors in the monotherapy setting. Common adverse events reported in PARP inhibitor monotherapy clinical trials include cytopenias related to BM toxicity such as anemia, thrombocytopenia, and neutropenia (17–22). A well-validated method to model such toxicity is *ex vivo* colony formation assays using hematopoietic progenitors derived from human BM. We evaluated the cytotoxic potency of veliparib, olaparib, talazoparib, rucaparib, and A-935935 toward erythroid and myeloid progenitors. The IC_{50}s for each of the clinical stage compounds fell within range of plasma exposures reported in monotherapy clinical trials at the recommended phase II doses (RP2D, Supplementary Table S2), highlighting the relevance of this approach to model a clinically relevant toxicity associated with this class of inhibitors. Comparison of IC_{50}s for PARP catalytic inhibition in BM mononuclear cells (BMN) shows a 40-fold difference between the most potent and least potent PARP inhibitors, whereas the IC_{50} differences for BMN cytotoxicity were greater than 600-fold (Supplementary Tables S3 and S4). These relative differences generally reflect those observed in cancer cell lines treated with alkylating agents (7–9). As has been reported for PARP trapping activity, different compounds displayed significant variation in the resolution between catalytic inhibition and BM toxicity. For veliparib, olaparib, rucaparib, and A-935935, the resolution between PAR inhibition and cytotoxicity spans >100-fold, but for the potent trapping agent talazoparib, there was less than a 2-fold difference between IC_{50}s for PAR inhibition and BMN cytotoxicity (Fig. 4; Supplementary Table S3). Strikingly, talazoparib was 73-fold and 26-fold more potent at killing hematopoietic progenitor cells than rucaparib and A-934935, respectively. These results suggest that PARP1 trapping activity is a primary driver of BM toxicity associated with single-agent PARP inhibition and that PARP inhibitors will differ in their ability to achieve robust catalytic inhibition in the absence of such toxicity.

To better understand the relationship between trapping and therapeutic index under monotherapy conditions, we compared the cytotoxicity of veliparib, olaparib, talazoparib, rucaparib, and A-934935 in a panel of cancer cell lines relative to BM (Fig. 5). Talazoparib is significantly more potent than all other compounds in every cell line tested, suggesting that PARP1 trapping contributes significantly to its single-agent activity in most contexts. However, all of the PARP inhibitors had similar patterns of cytotoxicity induction in the different cell lines. HeyA8 and DLDwt cells are relatively insensitive to all of the PARP inhibitors, whereas in DLD *BRCA2*$^{-/-}$ cells, all the PARP inhibitors had IC_{50}s that were below the IC_{50}s in BMN cells (Fig. 5A). As reported previously (23, 24), small cell lung cancer (SCLC) lines are more sensitive to PARP inhibition, as demonstrated by lower cytotoxicity IC_{50}s for all the PARP inhibitors in the SCLC lines (Fig. 5B) relative to HeyA8 and DLD1 cells. Synthetic lethality occurred in the breast cancer cells lines containing *BRCA* mutations, SUM149PT and MDA-MB-436, which were killed at much lower concentrations than the wild-type breast cancer lines (Fig. 5C). The ratio of cytotoxic potency in BM to cytotoxic potency in a given cancer cell line is comparable for all compounds tested, suggesting that the therapeutic index of a PARP inhibitor in the monotherapy setting may be independent of its trapping potency. This is reflective of preclinical data we previously reported for a combination regimen with TMZ (9).

Published OnlineFirst November 14, 2018; DOI: 10.1158/1541-7786.MCR-18-0138

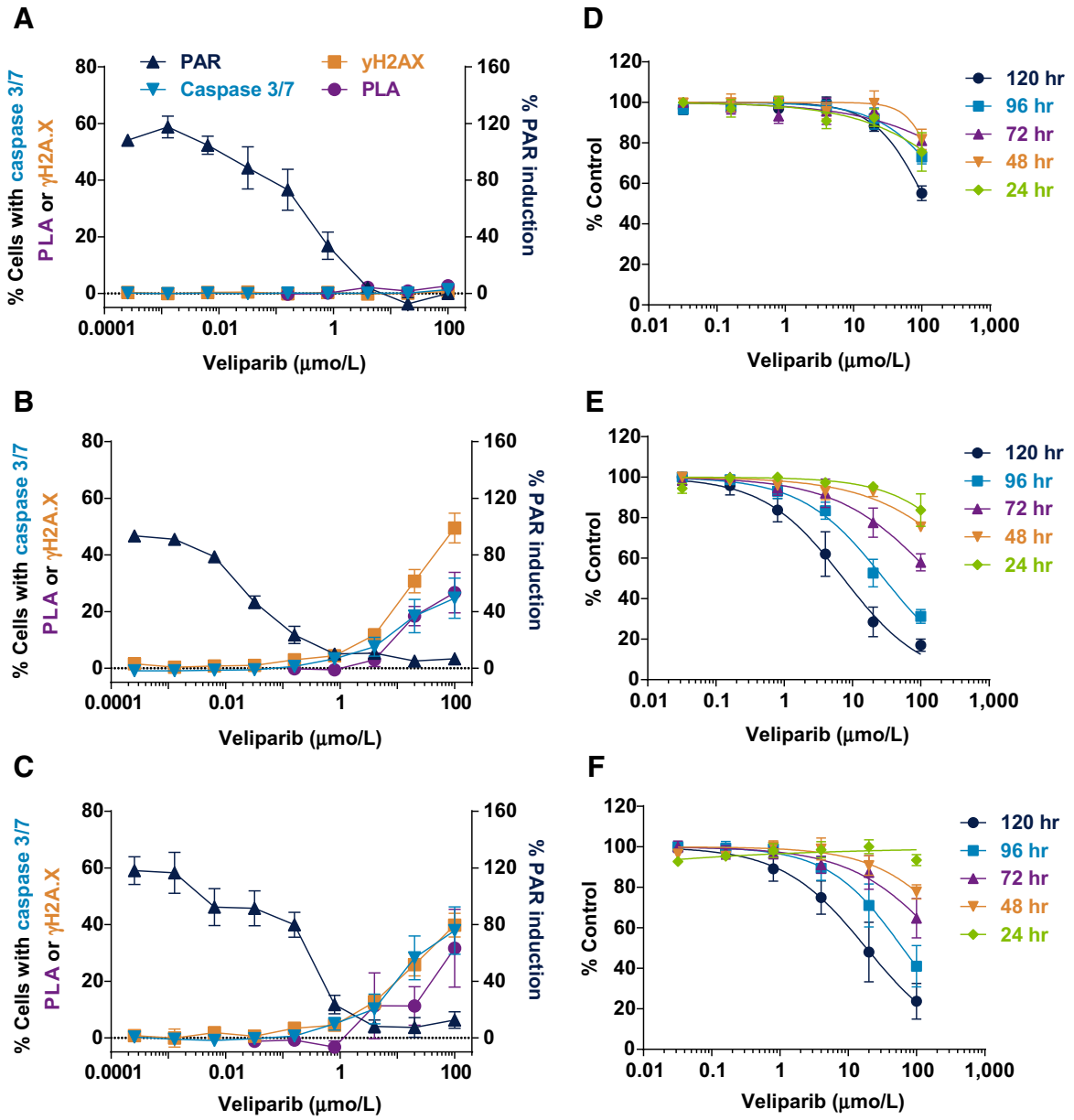

Figure 3.

PARP1 trapping induced by veliparib can be detected by PLA in *BRCA1* and *BRCA2* synthetic lethal cell line models. Dose-dependent inhibition of auto-PARylation (black line) and dose-dependent increased activation of apoptosis marker caspase 3/7 (blue), DNA damage marker γH2A.X (orange), and PLA (purple) in DLDwt (**A**), DLD *BRCA2*$^{-/-}$ (**B**), and SUM149PT (**C**). Time- and dose-dependent cytotoxicity induced by veliparib in DLDwt (**D**), DLD *BRCA2*$^{-/-}$ (**E**), and SUM149PT (**F**). Data are presented as mean ± SEM from at least three independent experiments.

In vivo study comparing veliparib, olaparib, rucaparib, and talazoparib in SUM149PT

We next extended the analysis of efficacy of PARP inhibitors with different trapping potencies to the *in vivo* setting. Mice bearing flank SUM149PT xenografts were treated for 42 days with the MTDs of veliparib, olaparib, and talazoparib (Fig. 6). Modest but significant tumor growth inhibition was exhibited in groups treated with all of the PARP inhibitors. Veliparib, olaparib, and talazoparib treatment resulted in 29%, 32%, and 35% growth delay, respectively (Fig. 6A). No weight loss or other adverse events were observed for all of the dosing groups (Fig. 6A). To determine whether compounds reached sufficient levels to inhibit PARP in the plasma and tumors, a parallel pharmacokinetics/pharmacodynamics (PK/PD) study in mice bearing SUM149PT xenografts was performed. Mice were treated for 5 days with the same dose and schedule for each PARP inhibitor that was used for the efficacy study. Plasma and tumor samples were collected at 1, 4, 24, 32, and 48 hours after the last dose, and compound and PAR levels were measured. Veliparib- and olaparib-treated tumors had >99% inhibition, and talazoparib-treated tumors had 94%

Published OnlineFirst November 14, 2018; DOI: 10.1158/1541-7786.MCR-18-0138

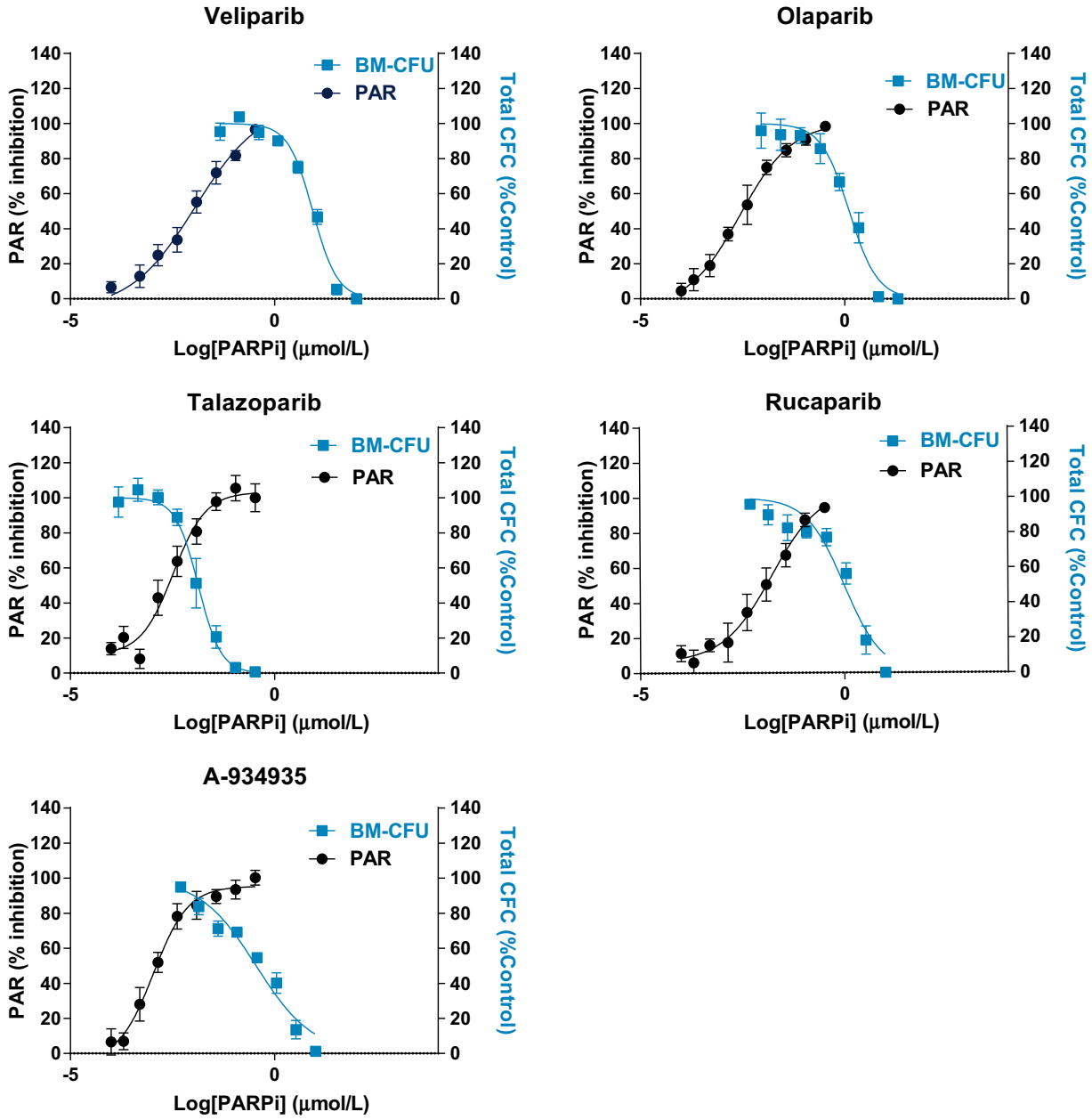

Figure 4.

PARP inhibitors differ in their resolution between catalytic inhibition and BM toxicity. BM colony-forming cell (CFC) data were normalized to DMSO controls and are presented as mean with standard errors of total CFCs (erythroid and myeloid lineages) from three independent donors. Cellular PAR levels were determined by ELISA in BM mononuclear cells treated with PARP inhibitors. Data are mean ± SEM from at least four independent experiments.

inhibition of PAR formation at 1 hour after the last dose of compound (Fig. 6B). PAR levels partially recovered at 4 hours and continued to increase over the rest of the time course. Recovery of PAR formation appeared faster for talazoparib compared with veliparib and olaparib. Although compound concentrations were below the limit of quantification in plasma for talazoparib after 4 hours, tumor compound levels decreased more slowly, with only a 65% decrease at 24 hours and 82% at 48 hours. Compound concentrations in the plasma were not detectible after 24 hours for veliparib and olaparib. Tumor levels for these compounds were still detectible at 48 hours, but the levels at 24 and 48 hours were decreased by 97% and 99% for veliparib and 96% and 98% for olaparib.

Discussion

Although PARP trapping has only been demonstrated in cells treated with combinations of PARP inhibitors and high concentrations of temozolomide or MMS (7–9), it is also hypothesized to be important for the single-agent activity of PARP inhibitors

Published OnlineFirst November 14, 2018; DOI: 10.1158/1541-7786.MCR-18-0138

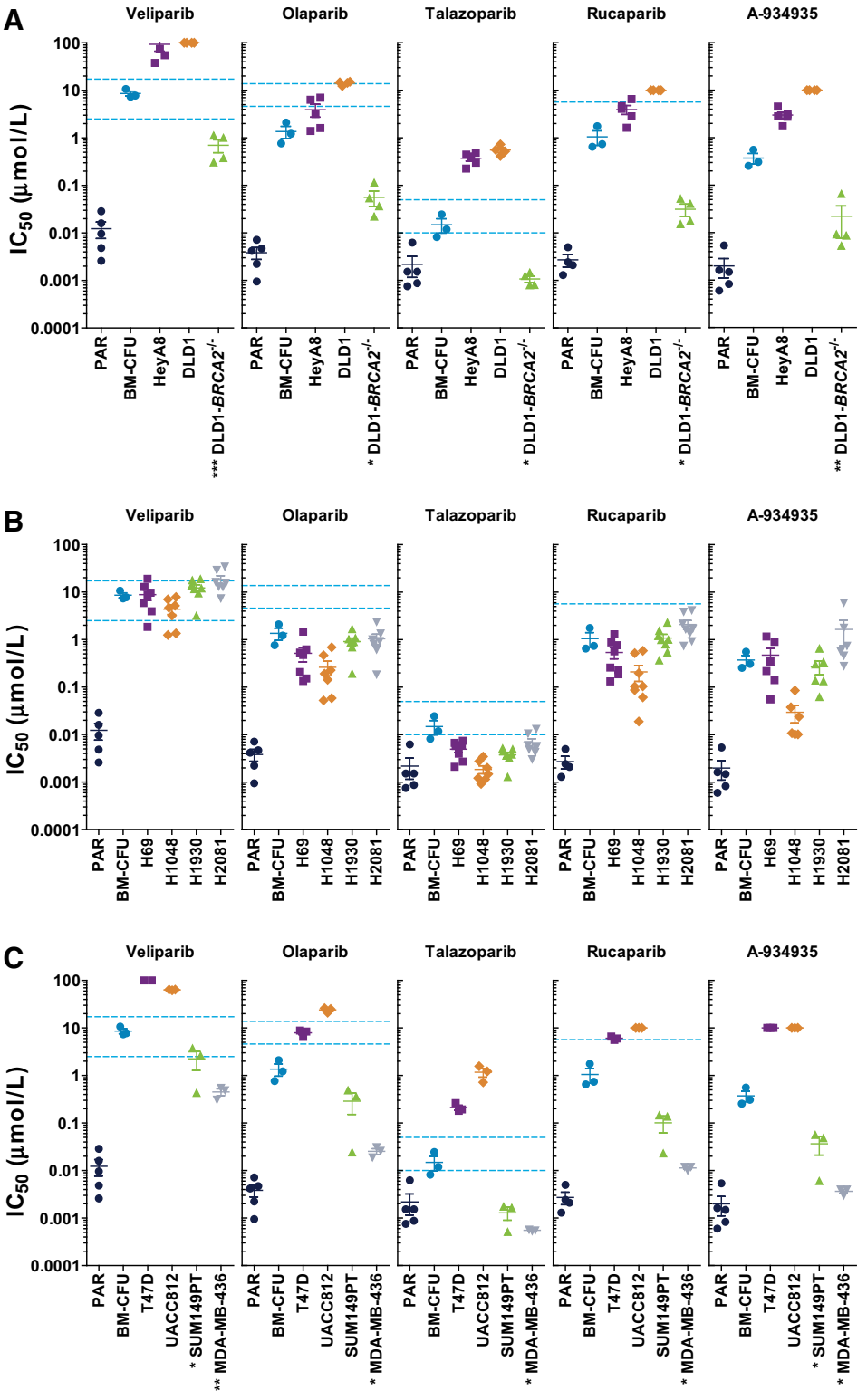

Figure 5.
PARP1 trapping activity is associated with greater *in vitro* cytotoxic potency toward multiple cancer cell lines. *In vitro* cytotoxic IC_{50}s of PARP inhibitors across cancer cell lines compared with inhibition of PAR formation and inhibition of colony formation of BM cells. IC_{50}s for HeyA8, DLD1, and DLD1 *BRCA2*$^{-/-}$ cells (**A**), SCLC lines (**B**), and breast cancer cell lines (**C**). For cell lines more sensitive than BM, a two-sided Student *t* test was performed and *, $P < 0.05$; **, $P < 0.01$; ***, $P < 0.001$. Dashed lines are clinical $C_{max/min}$ at monotherapy RP2D. Data points are from a minimum of three independent experiments, and mean ± SEM are indicated.

(6). Previously, there have only been correlative data supporting the hypothesis that PARP1 trapping plays a key role in cytotoxicity from PARP inhibitor monotherapy. Published methods (i.e., chromatin fractionation and Western blot) are not sensitive enough to detect endogenous PARP1 trapping in the monotherapy setting or trapping at clinically relevant exposures of temozolomide (9). Development of a PLA utilizing PARP1 and H2A.X has provided a 96-well–based assay with sufficient sensitivity to measure PARP1 trapping induced by PARP inhibitor/alkylating agent combinations as well as PARP inhibitor monotherapy

Published OnlineFirst November 14, 2018; DOI: 10.1158/1541-7786.MCR-18-0138

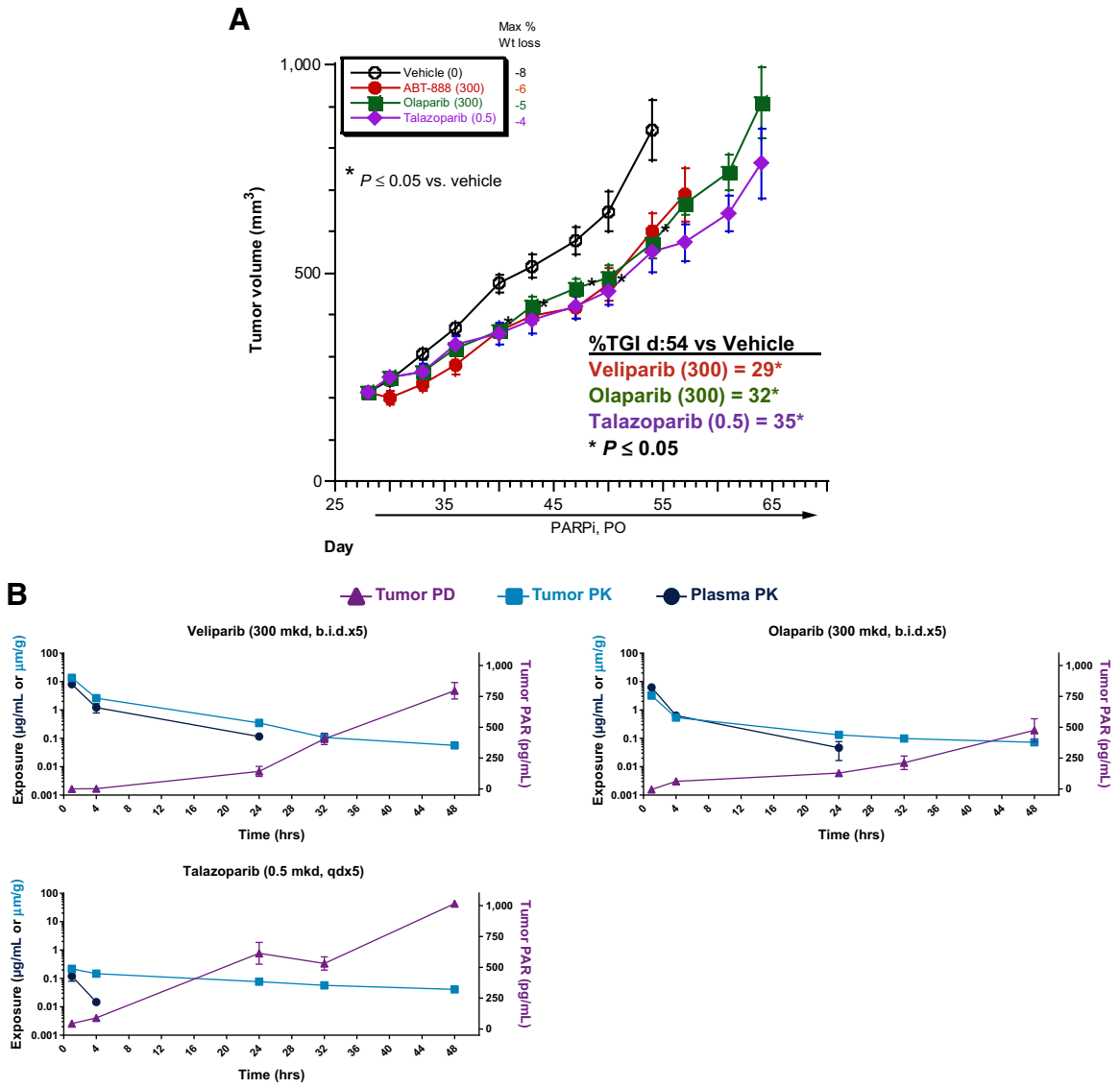

Figure 6.

Antitumor activity and PK/PD for veliparib, olaparib, and talazoparib in SUM149PT xenografts. **A,** Efficacy plots for SUM149PT xenografts in mice dosed p.o. with PARP inhibitors. PARP inhibitors were administered p.o., qd, or b.i.d. for 42 days (d30–71). Data are presented as mean with standard errors. Maximum percent weight loss and percent tumor growth inhibition (TGI) on day 54 vs. vehicle are indicated. *P* values are from two-sided *t* tests for mean difference in $\log_{10}$ (tumor volume) on specified day. **B,** PK and PD in SUM149PT xenograft tumor-bearing mice. Mice were dosed p.o., b.i.d., or qd as indicated with compounds for 5 days. At 1, 4, 24, 32, and 48 hours after the last dose, plasma and tumors samples were harvested. Plasma and tumor drug concentrations (PK) and tumor PAR levels (PD) were determined. Data are presented as mean with standard errors.

under endogenous cellular conditions. Because the Duolink PLA has been shown to work *in situ*, we propose that this methodology has potential application for evaluation of PARP trapping in clinical tumor samples.

The difference in trapping potency between talazoparib and other PARP inhibitors is up to 10,000-fold, whereas catalytic potency only differs by up to 40-fold (9). In order to better understand this difference, we characterized the trapping ability of two additional PARP inhibitors with PARP1 binding and catalytic potencies equal to talazoparib. Data from these studies showed that talazoparib is a more potent trapping agent than otherwise equipotent PARP inhibitors, with the following rank order of PARP1 trapping: talazoparib >> A-934935 = rucaparib (Fig. 1D). Based on these and previous data (9), talazoparib is unique in that its catalytic inhibition and trapping activities are not resolved. All other PARP inhibitors evaluated trap only at concentrations much higher than those required to inhibit PAR synthesis. Further studies are needed to identify the mechanism underlying the enhanced trapping potency of talazoparib.

Trapping contributes significantly to monotherapy activity of PARP inhibitors. The rank order of trapping potency for clinical PARP inhibitors in HeyA8 cells treated with 1 mmol/L MMS is talazoparib >> olaparib = rucaparib > veliparib = niraparib. The

Published OnlineFirst November 14, 2018; DOI: 10.1158/1541-7786.MCR-18-0138

same rank order is observed when comparing the cytotoxic potency for PARP inhibitor monotherapy treatment in HeyA8, DLD1, and DLD1-*BRCA2*$^{-/-}$ cells as well as SCLC and breast cancer lines. Our *in vitro* data indicate that PARP trapping is toxic to cancer cells with HRD, cancer cells with normal HR capacity, and normal cells (i.e., healthy human BM). *In vivo*, we observed comparable tumor growth inhibition at MTD in SUM149PT xenograft models with PARP inhibitors spanning a broad range of trapping potency. Together, these data suggest that the impact of trapping potency on the therapeutic index of PARP inhibitors in the monotherapy setting may be negligible.

Consistent with this hypothesis, currently available clinical data reveal no discernible relationship between trapping potency and monotherapy activity. Plasma exposures in patients treated with different PARP inhibitors at recommended phase 2 doses (Supplementary Table S1) appear inversely related to trapping potency. In addition, although veliparib is among the least efficient PARP trapping agents, in study NCI-2011-01472, evaluating veliparib monotherapy in *BRCA1/2*-mutated solid tumors, the overall RECIST response rate (PR + CR) was 40% among the 28 subjects who received at least 400 mg b.i.d. (25). Likewise, in the phase II portion of the Veli-BRCA study, an overall response rate of 47% was observed in 32 heavily pretreated (median 4 lines of prior therapy) patients with platinum-resistant or partially platinum-sensitive *gBRCA*-mutated epithelial ovarian cancer (26). These response rates are similar to those reported for olaparib (46% in platinum-sensitive ovarian cancer; ref. 27), niraparib (40% in *gBRCA*-mutated ovarian cancer; ref. 28), and talazoparib (42% in *gBRCA*-mutated ovarian cancer; ref. 17).

Although trapping potency may not have a significant bearing on monotherapy activity of PARP inhibitors in the clinic, our discovery that PARP1 trapping is a key driver of BM toxicity may be important for combination regimens including DNA-damaging chemotherapy that also induces BM toxicity. Here, we have shown that veliparib kills erythroid and myeloid progenitors only at concentrations well above those required to elicit robust inhibition of PAR synthesis. Consistent with this, recent data from a randomized phase II study indicate that doses of veliparib (120 mg b.i.d.) that are several fold higher than those required to inhibit PAR synthesis in patient tumors (29) can be combined with carboplatin at AUC6 and paclitaxel (200 mg/m2, q3wk) without exacerbation of cytopenias associated with the chemotherapy backbone (30). In contrast, our data reveal that talazoparib is toxic to erythroid and myeloid progenitors at concentrations similar to those required to inhibit PAR synthesis. Of note, recent clinical data indicate that combination of talazoparib with carboplatin at AUC1.5 results in significant enhancement of hematologic toxicity (31).

In conclusion, we have developed a novel methodology to demonstrate directly for the first time PARP1 trapping in cells treated with PARP inhibitors alone. We demonstrate that PARP inhibitors spanning a broad range of trapping potency elicit comparable monotherapy activity in a xenograft model of *BRCA*-mutant breast cancer, and that PARP1 trapping activity is a primary driver of toxicity of PARP inhibitors toward healthy BM progenitor cells. Contrary to recent suggestions (6), trapping activity appears unable to predict monotherapy clinical efficacy of PARP inhibitors; however, potent trapping agents may prove difficult to combine with DNA-damaging chemotherapy.

Disclosure of Potential Conflicts of Interest

V.C. Abraham reports receiving commercial research grant from AbbVie R& D funding and has an ownership interest (including stock, patents, etc.) in AbbVie. M.A. Algire, D. Maag, and J.L. Wilsbacher have an ownership interest (including stock, patents, etc.) in AbbVie. E.F. Johnson is Project Leader Oncology Development at, and has an ownership interest (including stock, patents, etc.) in, AbbVie. No potential conflicts of interests were disclosed by the other authors.

Authors' Contributions

Conception and design: T.A. Hopkins, V.C. Abraham, Y. Shi, E.F. Johnson, J.L. Wilsbacher, D. Maag

Development of methodology: T.A. Hopkins, W.B. Ainsworth, Y. Shi, D. Maag

Acquisition of data (provided animals, acquired and managed patients, provided facilities, etc.): T.A. Hopkins, W.B. Ainsworth, P.A. Ellis, E.L. DiGiammarino, S.C. Panchal, V.C. Abraham, M.A. Algire, Y. Shi, D. Maag

Analysis and interpretation of data (e.g., statistical analysis, biostatistics, computational analysis): T.A. Hopkins, W.B. Ainsworth, E.L. DiGiammarino, S.C. Panchal, V.C. Abraham, M.A. Algire, Y. Shi, A.M. Olson, J.L. Wilsbacher, D. Maag

Writing, review, and/or revision of the manuscript: T.A. Hopkins, W.B. Ainsworth, V.C. Abraham, M.A. Algire, Y. Shi, A.M. Olson, E.F. Johnson, J.L. Wilsbacher, D. Maag

Administrative, technical, or material support (i.e., reporting or organizing data, constructing databases): T.A. Hopkins, Y. Shi

Study supervision: T.A. Hopkins, J.L. Wilsbacher, D. Maag

Acknowledgments

The authors thank Don Osterling for helpful comments and discussion during the preparation of this article. Biochemical PARP assays were conducted by BPS Bioscience Inc. Bone marrow colony formation assays were conducted by Stemcell Technologies Canada, Inc.

This work was financially supported by AbbVie, Inc.

The costs of publication of this article were defrayed in part by the payment of page charges. This article must therefore be hereby marked *advertisement* in accordance with 18 U.S.C. Section 1734 solely to indicate this fact.

Received February 14, 2018; revised August 31, 2018; accepted October 23, 2018; published first November 14, 2018.

References

1. Lord CJ, Ashworth A. PARP inhibitors: synthetic lethality in the clinic. Science 2017;355:1152–8.
2. Scott LJ. Niraparib: first global approval. Drugs 2017;77:1029–34.
3. Karlberg T, Langelier MF, Pascal JM, Schuler H. Structural biology of the writers, readers, and erasers in mono- and poly(ADP-ribose) mediated signaling. Mol Aspects Med 2013;34:1088–108.
4. Ogata N, Ueda K, Kawaichi M, Hayaishi O. Poly(ADP-ribose) synthetase, a main acceptor of poly(ADP-ribose) in isolated nuclei. J Biol Chem 1981;256:4135–7.
5. Satoh MS, Lindahl T. Role of poly(ADP-ribose) formation in DNA repair. Nature 1992;356:356–8.
6. Pommier Y, O'Connor MJ, de Bono J. Laying a trap to kill cancer cells: PARP inhibitors and their mechanisms of action. Sci Transl Med 2016;8:362ps17.
7. Murai J, Huang SY, Das BB, Renaud A, Zhang Y, Doroshow JH, et al. Trapping of PARP1 and PARP2 by clinical PARP inhibitors. Cancer Res 2012;72:5588–99.
8. Murai J, Huang SY, Renaud A, Zhang Y, Ji J, Takeda S, et al. Stereospecific PARP trapping by BMN 673 and comparison with olaparib and rucaparib. Mol Cancer Ther 2014;13:433–43.
9. Hopkins TA, Shi Y, Rodriguez LE, Solomon LR, Donawho CK, DiGiammarino EL, et al. Mechanistic dissection of PARP1 trapping and

Published OnlineFirst November 14, 2018; DOI: 10.1158/1541-7786.MCR-18-0138

the impact on in vivo tolerability and efficacy of PARP inhibitors. Mol Cancer Res 2015;13:1465–77.
10. Murai J, Zhang Y, Morris J, Ji J, Takeda S, Doroshow JH, et al. Rationale for poly(ADP-ribose) polymerase (PARP) inhibitors in combination therapy with camptothecins or temozolomide based on PARP trapping versus catalytic inhibition. J Pharmacol Exp Ther 2014;349:408–16.
11. Webber SE, Canan-Koch SS, Tikhe J, Thoresen LH. Agouron Pharmaceuticals, Inc/Cancer Research Campaign Technology Limited. Tricyclic Inhibitors of Poly(ADP-ribose)Polymerases. United States patent US 6495541. 2000.
12. Penning TD, Zhu G, Gandhi VB, Gong J, Giranda VL. Pyrazoloquinolones are potent PARP inhibitors. United States patent US 8546368. 2013.
13. Ji J, Kinders RJ, Zhang Y, Rubinstein L, Kummar S, Parchment RE, et al. Modeling pharmacodynamic response to the poly(ADP-Ribose) polymerase inhibitor ABT-888 in human peripheral blood mononuclear cells. PLoS One 2011;6:e26152.
14. Kummar S, Chen A, Ji J, Zhang Y, Reid JM, Ames M, et al. Phase I study of PARP inhibitor ABT-888 in combination with topotecan in adults with refractory solid tumors and lymphomas. Cancer Res 2011;71:5626–34.
15. Kummar S, Kinders R, Gutierrez ME, Rubinstein L, Parchment RE, Phillips LR, et al. Phase 0 clinical trial of the poly (ADP-ribose) polymerase inhibitor ABT-888 in patients with advanced malignancies. J Clin Oncol 2009;27:2705–11.
16. Kikuchi R, Lao Y, Bow DA, Chiou WJ, Andracki ME, Carr RA, et al. Prediction of clinical drug-drug interactions of veliparib (ABT-888) with human renal transporters (OAT1, OAT3, OCT2, MATE1, and MATE2K). J Pharm Sci 2013;102:4426–32.
17. de Bono J, Ramanathan RK, Mina L, Chugh R, Glaspy J, Rafii S, et al. Phase I, dose-escalation, two-part trial of the PARP inhibitor talazoparib in patients with advanced germline BRCA1/2 mutations and selected sporadic cancers. Cancer Discov 2017;7:620–9.
18. Konecny GE, Kristeleit RS. PARP inhibitors for BRCA1/2-mutated and sporadic ovarian cancer: current practice and future directions. Br J Cancer 2016;115:1157–73.
19. Kristeleit R, Shapiro GI, Burris HA, Oza AM, LoRusso P, Patel MR, et al. A phase I-II study of the oral PARP inhibitor rucaparib in patients with germline BRCA1/2-mutated ovarian carcinoma or other solid tumors. Clin Cancer Res 2017;23:4095–106.
20. Domchek SM, Aghajanian C, Shapira-Frommer R, Schmutzler RK, Audeh MW, Friedlander M, et al. Efficacy and safety of olaparib monotherapy in germline BRCA1/2 mutation carriers with advanced ovarian cancer and three or more lines of prior therapy. Gynecol Oncol 2016;140:199–203.
21. Coleman RL, Sill MW, Bell-McGuinn K, Aghajanian C, Gray HJ, Tewari KS, et al. A phase II evaluation of the potent, highly selective PARP inhibitor veliparib in the treatment of persistent or recurrent epithelial ovarian, fallopian tube, or primary peritoneal cancer in patients who carry a germline BRCA1 or BRCA2 mutation - an NRG Oncology/Gynecologic Oncology Group study. Gynecol Oncol 2015;137:386–91.
22. Mirza MR, Monk BJ, Herrstedt J, Oza AM, Mahner S, Redondo A, et al. Niraparib maintenance therapy in platinum-sensitive, recurrent ovarian cancer. N Engl J Med 2016;375:2154–64.
23. Byers LA, Wang J, Nilsson MB, Fujimoto J, Saintigny P, Yordy J, et al. Proteomic profiling identifies dysregulated pathways in small cell lung cancer and novel therapeutic targets including PARP1. Cancer Discov 2012;2:798–811.
24. Cardnell RJ, Feng Y, Diao L, Fan YH, Masrorpour F, Wang J, et al. Proteomic markers of DNA repair and PI3K pathway activation predict response to the PARP inhibitor BMN 673 in small cell lung cancer. Clin Cancer Res 2013;19:6322–8.
25. Puhalla S, Beumer JH, Pahuja S, Appleman LJ, Tawbi HAH, Stoller RG, et al. Final results of a phase 1 study of single-agent veliparib (V) in patients (pts) with either BRCA1/2-mutated cancer (BRCA+), platinum-refractory ovarian, or basal-like breast cancer (BRCA-wt). J Clin Oncol 2014;32(15_suppl):2570.
26. Steffensen KD, Adimi P, Jakobsen AKM. Veliparib monotherapy to patients with BRCA germline mutation and platinum-resistant or partially platinum-sensitive selapse of epithelial ovarian cancer: a phase I/II study. J Clin Oncol 2016;34(15_suppl):5532.
27. Fong PC, Yap TA, Boss DS, Carden CP, Mergui-Roelvink M, Gourley C, et al. Poly(ADP)-ribose polymerase inhibition: frequent durable responses in BRCA carrier ovarian cancer correlating with platinum-free interval. J Clin Oncol 2010;28:2512–9.
28. Sandhu SK, Schelman WR, Wilding G, Moreno V, Baird RD, Miranda S, et al. The poly(ADP-ribose) polymerase inhibitor niraparib (MK4827) in BRCA mutation carriers and patients with sporadic cancer: a phase 1 dose-escalation trial. Lancet Oncol 2013;14:882–92.
29. LoRusso PM, Li J, Burger A, Heilbrun LK, Sausville EA, Boerner SA, et al. Phase I safety, pharmacokinetic, and pharmacodynamic study of the poly (ADP-ribose) polymerase (PARP) inhibitor veliparib (ABT-888) in combination with irinotecan in patients with advanced solid tumors. Clin Cancer Res 2016;22:3227–37.
30. Ramalingam SS, Blais N, Mazieres J, Reck M, Jones CM, Juhasz E, et al. Randomized, placebo-controlled, phase II study of veliparib in combination with carboplatin and paclitaxel for advanced/metastatic non-small cell lung cancer. Clin Cancer Res 2017;23:1937–44.
31. Dhawan MS, Bartelink IH, Aggarwal RR, Leng J, Kelley RK, Melisko ME, et al. A phase I study of carboplatin and talazoparib in patients with and without DNA repair mutations. J Clin Oncol 2017;35 (15_suppl):2527.

AACR American Association for Cancer Research

Molecular Cancer Research

PARP1 Trapping by PARP Inhibitors Drives Cytotoxicity in Both Cancer Cells and Healthy Bone Marrow

Todd A. Hopkins, William B. Ainsworth, Paul A. Ellis, et al.

Mol Cancer Res Published OnlineFirst November 14, 2018.